Unraveling Global Microwave Signatures and Changes of Snowfall Over Cold Land Surfaces

Zeinab Takbiri, Sagar Tamang, Ardeshir Ebtehaj, Efi Foufoula-Georgiou

University of Minnesota "Driven to Discover℠"

UC Irvine

Goal and Motivation

- The goals are (1) better understand the microwave radiometric signatures of snowfall over snow-covered surfaces and (2) characterize the changes of global snowfall data in the past 40 years.
- The objectives are:
  1) Quantify microwave interaction of snow and snowfall.
  2) Quantify microwave interaction of the liquid water path and snowfall.
  3) Unmix the snow cover and the cloud liquid water signals from snowfall scattering signal.
  4) Use the reanalysis wet bulb temperature and GPCP to quantify global transition of snowfall to rainfall dominant regimes.

SWE and GPM Brightness Temperatures

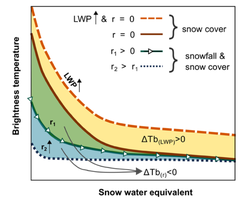

Figure 1: A schematic of the generic effects of snow cover and cloud LWP on snowfall high-frequency microwave signal as a function of the snow water equivalent (SWE).

In particular, we try to address the following main questions:

- What are the scattering contributions of snowfall and snow cover in decreased brightness temperatures for different snowfall intensity and snow-cover depth?
- Why, when, where and to what extent the liquid water content of snowy clouds can mask the snowfall signals over snow-covered surfaces?
- Under which boundary conditions can the snow cover obscure the snowfall signatures?
- Is there any blind boundary conditions for microwave snowfall retrievals?

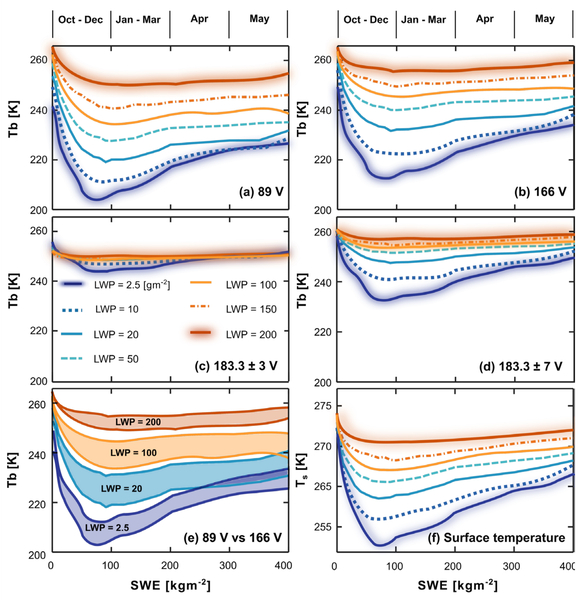

Figure 2: Variations of brightness temperatures at GPM frequency channel 89v (a), 166v (b), 183±3 (c), and 183±7 (d) GHz, the difference between the Tb responses of channel 89 and 166 GHz to LWP (e), and variations of surface temperature against the snow water equivalent (SWE, f).

- High-frequency GMI Tbs do not monotonically decrease as SWE increase and approach a minimum for SWE values around 70 kgm^{-2} and then begin to increase.
- The observed anomaly follows the climatology of snow-cover temperature for different SWE values. The main reason is that the snow cover temperature and its metamorphic changes of grain size are not independent.

The Snow Cover Scattering Under Clear Sky

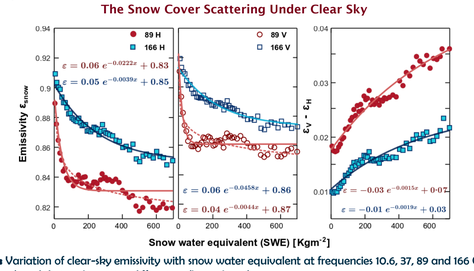

Figure 3: Variation of clear-sky emissivity with snow water equivalent at frequencies 10.6, 37, 89 and 166 GHz (first two columns) and their polarization differences (last column).

Note that the total cloud liquid water path, integrated precipitable liquid, and ice water column of the atmosphere, and the near-surface precipitation are all zeros based on the data from MERRA model simulations and DPR ancillary data (2ADPR-ENV).

Snowfall Signatures for different SWE and LWP

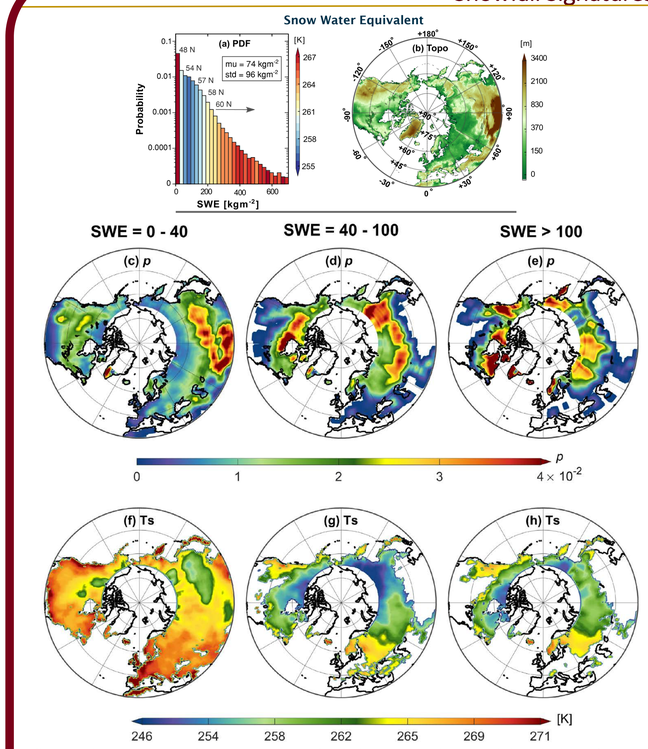

Figure 4: The global variation of snow water equivalent (SWE). The marginal and spatial probability distribution function (PDF) of annual Snow Water Equivalent (SWE) and its surface temperature (T_s), using the MERRA data from 2014 to 2017. The marginal PDF of SWE and its corresponding surface temperature (a), the NH topographic map (b), the SWE spatial probability of occurrence p (c-e), and the snow-cover surface temperature Ts (f-h) at 1 degree resolution for three SWE intervals.

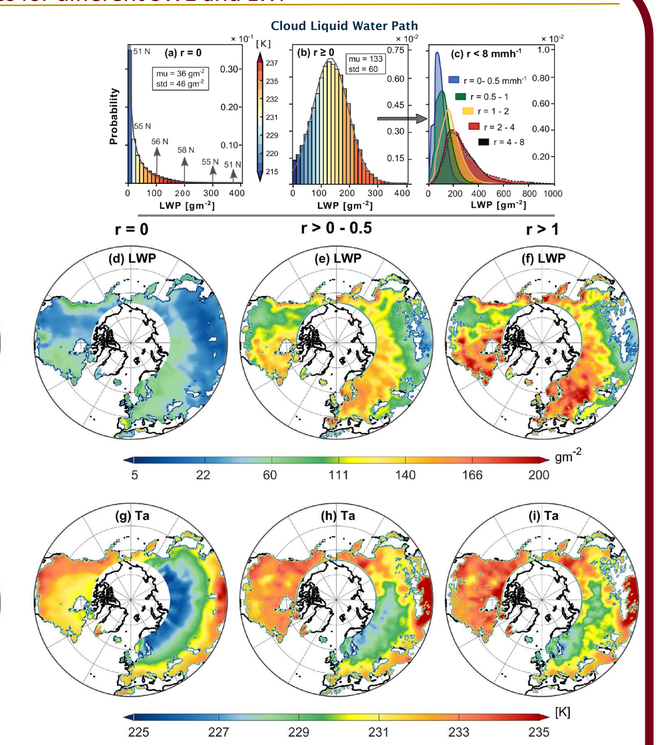

Figure 5: The effects of different overland snowfall rates on frequency and spatial distribution of the cloud liquid water path (LWP) over the NH. The probability distribution function of LWP for different values of snowfall (a-c), the spatial distribution of the mean LWP (d-f), and mean vertical air temperature (g-i) for non-precipitating (r = 0) and snowing atmosphere (r > 0). The histograms are color coded to represent the corresponding mean air temperatures.

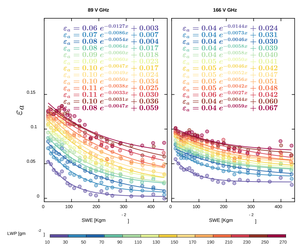

Figure 6: The atmospheric emissivity for different values of LWP over snow-covered surfaces.

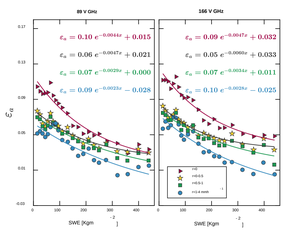

Figure 7: Atmospheric emissivity comparison of snowing cloud for LWP=150-160 gm-2.

- Over the SWE less than 70 kgm^{-2} and LWP <70 gm^{-2}, the light snowfall (<0.5 mmh^{-1}) scattering is detectable only at frequency 166 GHz. For higher intensities the signal can be also detected in 89 GHz.
- When SWE exceeds 200 kgm^{-2} and the LWP is >70 gm^{-2}, the emission from the increased LWP in snowing clouds becomes the only surrogate microwave signal of snowfall that is stronger at frequency 89 GHz than 166 GHz.
- Over high latitudes above 60° N where the SWE is larger than 200 kgm^{-2} and LWP is <70 gm^{-2}, there exists a blind zone over which the microwave signatures of light snowfall below 0.5 mmh^{-1} are totally obscured.

$$T_{obs} = Ts \times \varepsilon_{sc} + Ta \times \varepsilon_a \qquad \varepsilon_{sc}: Tb_{obs}\ (\text{of clear sky})\ /Ts$$

$$\varepsilon_a = (Tb_{obs} - Ts \times \varepsilon_{sc})/Ta$$

Ts: surface temperature
Ta: air temperature

Global Changes in Snowfall: A Transition from Snowfall to rainfall Dominant Regimes

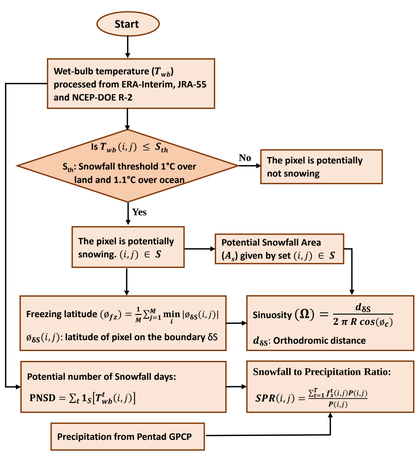

Figure 8: Schematic diagram of the used framework for analyzing changes in snowfall utilizing cumulative precipitation from Pentad GPCP and wet-bulb temperature from multiple reanalysis products.

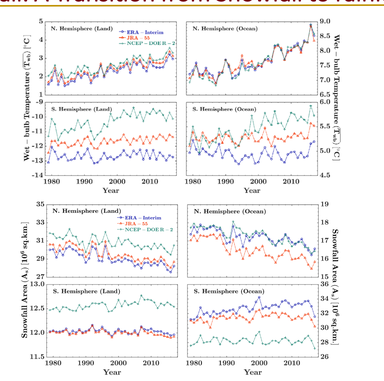

Figure 9: The time series of annual averaged wet-bulb temperature for the NH and the SH lands and oceans (top two rows). The time series of annual average potential snowfall area for NH and SH lands and oceans (bottom two rows).

Over NH lands (oceans), wet-bulb temperature increased annually at 0.32-0.35 (0.35-0.41)°C/decade with potential snowfall areas shrinking at 0.44-0.56 (0.28-0.39) million km^2/decade. Over SH lands, wet-bulb temperature increased at 0.04-0.41°C/decade with insignificant change in potential snowfall areas whereas over SH ocean, despite the insignificant change in average wet-bulb temperature, snowfall area is expanding at 0.03-0.53 million km^2/decade.

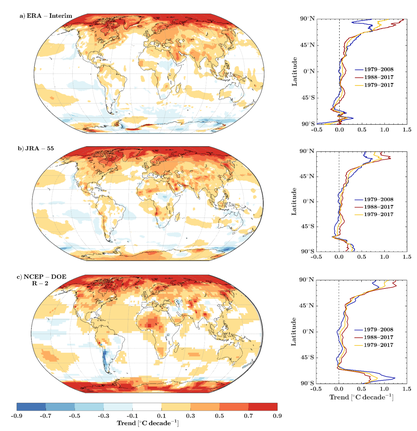

Figure 10: Trends in annual average wet-bulb temperature for (a) ERA-Interim, (b) JRA-55 and (c) NCEP-DOE R-2 (left column). The zonal trend in annual average wet-bulb temperature for the period of 1979–2008, 1988-2017 and 1979–2017 (right column).

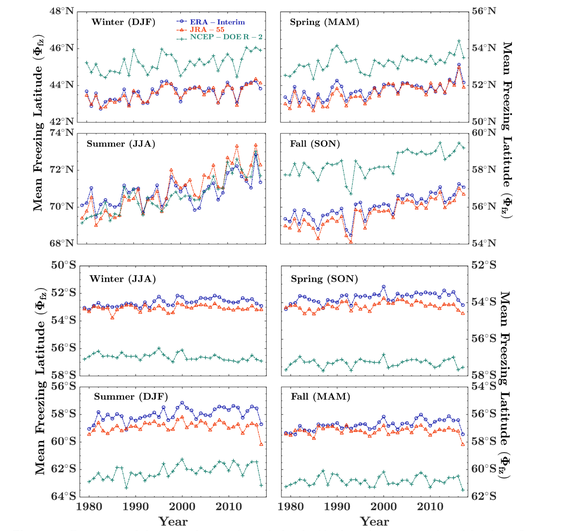

Figure 11: Time series of the mean freezing latitude for the Northern (top two rows) and Southern (bottom two rows) Hemisphere at winter, spring , summer and fall.

The NH snowfall area is shrinking with mean freezing latitude shifting at 0.32-0.47°/decade towards the North Pole whereas the SH snowfall area is expanding with mean freezing latitude shifting at 0.03-0.21°/decade towards the equator resulting in an overall expansion and northward shift of tropics.

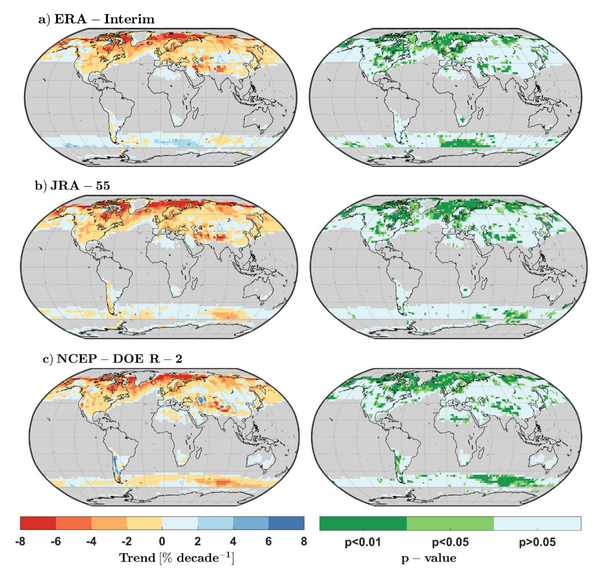

Figure 12: Trend in Snowfall to Precipitation Ratio (SPR) and its significance level. Important mountainous regions of the world including Himalayan Region, Swiss Alps, Andes Mountains and Rocky mountains are showing a significant transitioning of snowfall to rainfall dominant regimes at the rate of 2-4%/decade.

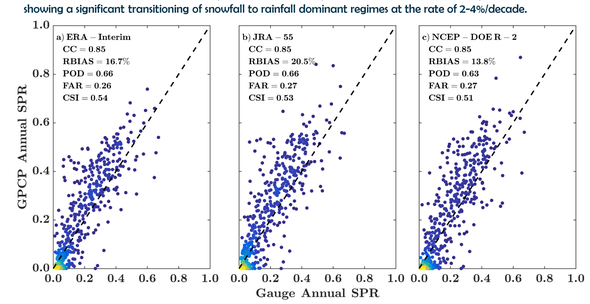

Figure 13: Validation of Annual SPR against ground based observations from 345 precipitation gauges provided by National Climatic Data Center during the period of 2014-2015. Results suggest that combination of wet-bulb temperature from ERA-Interim and Precipitation from Pentad GPCP performs the best with high CC and CSI and a low RBIAS and FAR.

Acknowledgment: This research is supported by two GPM grants GPM: NNX16AO56G and NIP: 80N55C18K0742

1- Ebtehaj, A.M., R.L. Bras, E. Foufoula-Georgiou (2015), "Shrunken locally linear embedding for passive microwave retrieval of precipitation", *IEEE Trans. on Geosci. and Remote Sens.*, vol 53(7), doi:10.1109/TGRS.2014.2382436.
2- Ebtehaj, A.M., R.L. Bras, E. Foufoula-Georgiou (2016), "Evaluation of ShARP passive rainfall retrievals over snow-covered land surfaces and coastal zones", *J. Hydrometeor*, 17, 1013–1029.doi:doi: http://dx.doi.org/10.1175/JHM-D-15-0164.1
3- A Prognostic Retrieval Approach for Microwave Precipitation Phase Detection over Snow Cover, Z. Takbiri, Ebtehaj A., E. Foufoula-Georgiou, P. Kirstetter, J. Turk, under review in JHM